IEEE Access
Multidisciplinary | Rapid Review | Open Access Journal

Received September 14, 2019, accepted September 27, 2019, date of publication October 2, 2019, date of current version October 15, 2019.

Digital Object Identifier 10.1109/ACCESS.2019.2945162

Soft-Switching Proximate Time Optimal Heading Control for Underactuated Autonomous Underwater Vehicle

AN LI, LI YE, JIANG YANQING, LI YUEMING, CAO JIAN, AND HE JIAYU
Science and Technology on Underwater Vehicles Laboratory, Harbin Engineering University, Harbin 150001, China

Corresponding authors: Li Ye (liyeheu103@163.com) and Cao Jian (caojian_heu@163.com)

This work was supported in part by the National Key Research and Development Program of China under Grant 2017YFC0305700, in part by the National Natural Science Foundation of China under Grant U1806228, Grant 51879057, Grant 51609047, and Grant 51809064, in part by the Fundamental Research Funds for the Central Universities under Grant HEUCFG201810, in part by the Qingdao National Laboratory for Marine Science and Technology under Grant QNLM2016ORP0406, and in part by the Research Fund for Science and Technology on Underwater Vehicles Laboratory under Grant 6142215180102.

ABSTRACT In this paper, a soft-switching proximate time-optimal control (PTOC) is proposed based on the model-compensation extended state observer (ESO) and Takagi–Sugeno fuzzy switching, for the fast set-heading tracking of underactuated autonomous underwater vehicle (AUV). First, based on Pontryagin's maximum principle, a time-optimal control (TOC) law is derived for the first-order Nomoto model of the underactuated AUV. Then, a model-compensation active disturbance rejection control (ADRC) is developed; the outstanding characteristic is that the nonlinear heading dynamic model is compensated to a first-order Nomoto model rather than by a double integral system through implementing a model-compensation ESO (MC-ESO). The regular ESO is replaced with a reduced-order ESO (RESO) to reduce complexity, and the model-compensation RESO (MC-RESO) is designed by adding the known partial model to RESO. Based on the controller scaling method, a parameter self-tuning strategy is proposed for model-compensation ADRC (MC-ADRC) with changed plant parameters at different velocities. Finally, the soft-switching PTOC is developed for heading control, and the MC-RESO is adopted to estimate the unmeasured velocity and unknown total disturbances for feedback and compensation. The TOC with an unsaturated region (RTOC) is employed to enhance the robustness by using a switching region to replace the switching curve, and a soft-switching strategy between ADRC (near the origin) and RTOC (far from origin) is designed based on the Takagi–Sugeno fuzzy mode. Several simulations are carried out, the effectiveness of self-tuning MC-ADRC is verified, and the proposed soft-switching PTOC shows better performance compared with MC-ADRC.

INDEX TERMS Underactuated autonomous underwater vehicle (AUV), heading control, model-compensation extended state observer (ESO), proximate time-optimal control (PTOC), fuzzy switching.

I. INTRODUCTION

Autonomous Underwater Vehicle (AUV) has been widely used in marine development. AUV play an important role in many fields, such as ocean salvage, deep sea resources exploration, ocean hydrological observation, ocean surveying, and submarine pipeline maintenance, and have broad application prospects in the military field [1]. At present, most AUV are underactuated, such as the Remus 6000, Bluefin-21, Autosub 6000, and HUGIN 4500. For the underactuated AUV control system, heading control is the basic means to guarantee that the underwater vehicle accomplishes particular tasks successfully [2]; moreover, heading control is directly related to the operation, safety, and effectiveness of the AUV's control system [3]. The AUV's dynamic system is nonlinear, uncertain, and time-varying [1]. Therefore, it is difficult to establish an accurate mathematical model. Additionally, achieving heading control of the underactuated AUV is difficult due to coupled nonlinearities [4], hydrodynamic coefficients change at different velocities [5], the limited rudder angle [6], and external disturbances such as ocean currents [7].

The associate editor coordinating the review of this manuscript and approving it for publication was Yougan Chen.

Various models of control techniques have been applied in underactuated AUV heading control. Many researchers have made great contributions, including the proportion integral derivative (PID) algorithm and various improved PID algorithms [8]–[10], SMC controllers [11], [12], self-adaptive fuzzy control [1], [13], adaptive control and hybrid control [2], [5], dynamic surface control [14], and artificial neural network control [15], [16]. However, most of the control methods remain in the theoretical study stage.

Recently, active disturbance rejection control (ADRC) has become quite attractive to applied researchers even though theoretical justification was lagging behind for quite some time because its uniqueness in concepts, simplicity in engineering implementation, and superior performance have been readily translated into something valuable in engineering practice [17]. ADRC [18] was originally proposed by Han in 1998, and has been successfully applied to numerous types of processes [19]. ADRC treats external disturbances and unknown internal dynamics as an extended state of the plant, and then estimates this state using an extended state observer (ESO) and compensates for it in real time. ADRC has found wide applications in underwater vehicle control, all the plant is compensated to double integral system by ESO [20]. In [21], Cui *et al* suggested that the boundedness assumption of the derivation of uncertainty for ESO would be violated because the uncertainty part is always involved with the velocities of the AUV. In order to deal with the large changes in system dynamics and disturbances, a model-compensation ESO was proposed in a previous study [22], and the strong robustness against uncertain dynamics and external disturbances was verified.

In some cases, there is a requirement that the underactuated AUV turns to a certain heading angle in the shortest time with input saturation constraints, such as in underwater docking and emergency obstacle avoidance. For point-to-point fast tracking with limited control signals, the theoretically best solution should be the time-optimal control (TOC), which applies the maximum control variable to achieve the fastest acceleration followed by braking. TOC is a bang-bang control scheme with respect to the time-optimal switching curve developed on the basis of the maximum principle [23]. Some research on time-optimal heading control of AUV has been carried out. In the second phase of underwater docking, Park *et al* adopted the time-optimal control (bang-bang) for AUV heading control to quickly eliminating the crab angle [24]. In [2], a BB-PID controller was designed for the heading control of AUV by utilizing the complementary advantages of bang-bang and the PID controller. The TOC heading control will lead to control chattering in the presence of plant uncertainties or disturbances. In order to avoid this chattering, the control law described in two previous studies [2], [24] transits into PID control or no control, respectively, when the heading error is less than the set threshold.

Recently, some improvements have been proposed for TOC. In order to overcome the shortcoming of TOC and enhance the robustness in practical application, adaptive proximate time-optimal servomechanism (PTOS) were proposed for continuous and discrete systems [25], [26], respectively. The PTOS approach modifies the time-optimal switching curve by including an unsaturated ''slab'' region, and smoothly transits into a linear control law for small errors [27]. Multiple studies have been conducted on the basis of the PTOS [28]–[30]. In [28], Young *et al* proposed a modification to the PTOS scheme where the feedback gains were updated based on a dynamically scheduled damping ratio. The dynamic damping control was introduced to PTOS [29], resulting in better performance. A robust PTOS control law has also been designed, and a reduced-order extended state observer (RESO) was adopted to estimate the unmeasured velocity and unknown disturbance for feedback and compensation [30].

All the aforementioned work for TOC assumed that the plant is a double-integrator model. In practice, the heading motion model of the underactuated AUV to be controlled more typically has a damping element to describe the acceleration process of angular velocity, i.e. the first-order Nomoto model. In 1975, the heading response equation of underactuated marine vehicles was analyzed by Nomoto using the automatic regulation principle, and then the first-order Nomoto model was put forward. Its simplicity and relative accuracy in describing the yaw dynamics has been verified [31]. Obviously, the aforementioned PTOC method cannot be directly applied to underactuated AUV heading control. Until now, there have been few studies aimed at the TOC of the plant model as an integrator cascaded with an inertia block. A previous study [32] demonstrates the representative results; proximate time-optimal control (PTOC) is extended to the more typical second-order servo systems with a damping element, and a parameterized design of expanded proximate time-optimal servomechanism control law with a speed-dependent linear region is presented for rapid and smooth set-point tracking using a bounded input signal.

Motivated by the above considerations and analysis, a soft-switching PTOC is proposed based on model-compensation ESO and the Takagi–Sugeno fuzzy mode for the fast set-heading tracking of the underactuated AUV. The main contributions of this paper can be summarized as follows:

1. The existing studies on time-optimal heading control of AUV only have some applications lacking strict theoretical deduction, and the switching of control signal is based on the set threshold rather than the TOC switching curve. In order to provide theoretical support, the time-optimal heading control law is, to our knowledge, the first to be derived for the underactuated AUV heading with a first-order Nomoto model based on Pontryagin's maximum principle.

2. A model-compensation ESO (MC-ESO) is first introduced to the heading dynamic. The main difference of MC-ESO compared to the general ESO is that the plant is compensated to a first-order Nomoto model rather than a double integral system; and the strong robustness against uncertain dynamics and external disturbances has been verified

in [22]. The parameters of the Nomoto model are directly related to the AUV's velocity. Therefore, in order to improve the adaptability of the controller at different velocities, a practical parameter self-tuning strategy is designed for the feedback controller using the controller scaling method.

3. In order to enhance the practical application of TOC, soft-switching PTOC is proposed for the heading control of underactuated AUV with unmodeled dynamics and external disturbances. Based on the TOC control law for the Nomoto model, the PTOC is designed by adding an unsaturated region to TOC, and smoothly transits into ADRC for small errors. The essential difference of soft-switching PTOC compared to the general PTOC is that the switching strategy of controllers is based on the Takagi–Sugeno fuzzy mode rather than a set constant threshold, which is obviously more reasonable and effective for different targets at different surge velocities.

The remainder of this paper is organized as follows. Section II formulates the TOC control problem for heading of the underactuated AUV. Section III presents the details for designing the soft-switching PTOC controller. In Section IV, the simulations are presented to verify the heading control strategy. The conclusions and some future work directions are given in Section V.

II. PROBLEM FORMULATION

A. DYNAMIC AND KINEMATIC MODEL FOR UNDERACTUATED AUV IN HORIZONTAL PLANE

The WL-3 AUV studied in this paper was developed by the Science and Technology on Underwater Vehicles Laboratory affiliated with Harbin Engineering University, China. As shown in Fig. 1, the WL-3 AUV is an underactuated autonomous underwater vehicle. The WL-3 AUV is a propeller-rudder-driven AUV, with the cruising velocity 2 kn (the input voltage of the propeller is 3 V) and maximum velocity 4 kn (the input voltage of the propeller is 5 V). The main parameters of the WL-3 AUV are shown in Table 1.

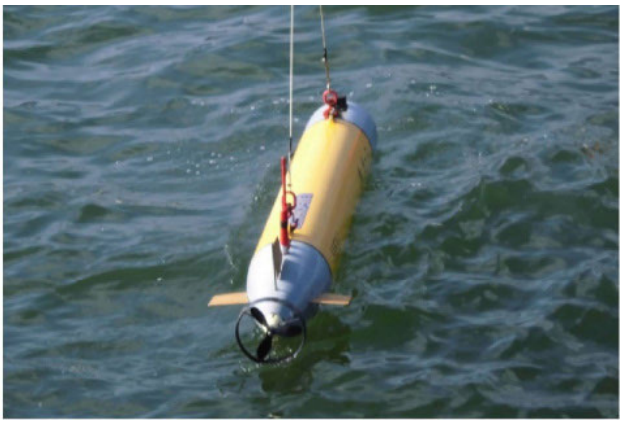

FIGURE 1. The WL-3 AUV.

The inertial reference coordinate system {**I**} is established with the Earth defined as the origin, and the body-fixed

TABLE 1. Parameters of the WL-3 AUV.

Parameters	Value	Parameters	Value
Length l	2550 mm	Diameter of the hull D	340 mm
Total weight m	183 kg	Operation depth	300 m
Inertia moment I_z	94.55 $kg \cdot m^2$	Actuators	propeller, rudders

TABLE 2. Dimensionless hydrodynamic coefficients of the WL-3 AUV.

Parameters	Value	Parameters	Value
$X'_{\dot{u}}$	$-1.578 \cdot 10^{-3}$	$X'_{u\|u\|}$	$-5.000 \cdot 10^{-3}$
X'_{vr}	$3.075 \cdot 10^{-2}$	X'_{rr}	$-9.420 \cdot 10^{-4}$
$Y'_{\dot{v}}$	$-3.075 \cdot 10^{-2}$	$Y'_{\dot{r}}$	$9.420 \cdot 10^{-4}$
$Y'_{v\|v\|}$	$-1.669 \cdot 10^{-1}$	$Y'_{r\|r\|}$	$1.258 \cdot 10^{-2}$
Y'_{r}	$2.216 \cdot 10^{-2}$	Y'_{v}	$-4.496 \cdot 10^{-2}$
$N'_{\dot{r}}$	$-1.601 \cdot 10^{-3}$	$N'_{\dot{v}}$	$1.060 \cdot 10^{-3}$
$N'_{v\|v\|}$	$6.91 \cdot 10^{-3}$	N'_{rr}	$-1.443 \cdot 10^{-3}$
N'_{r}	$-1.168 \cdot 10^{-2}$	N'_{v}	$-9.378 \cdot 10^{-3}$
$N'_{\|v\|r}$	$-2.516 \cdot 10^{-2}$		

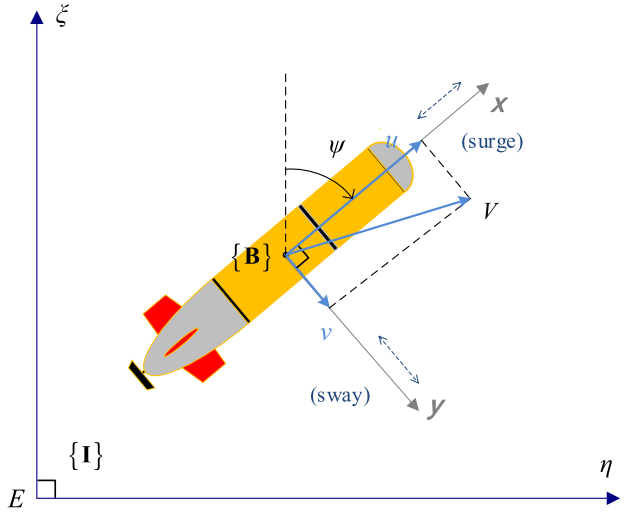

FIGURE 2. Coordinate system of the AUV in the horizontal plane.

reference {**B**} with the origin chosen to coincide with the center of mass of the AUV, as shown in Fig. 2.

The kinematic model of the AUV in the horizontal plane can be described as follows [23]:

$$\begin{aligned} \dot{\boldsymbol{\eta}} &= \mathbf{R}(\psi)\mathbf{v} \\ \boldsymbol{\eta} &= [x \quad y \quad \psi]^{\mathrm{T}}, \quad \mathbf{V} = [u \quad v \quad r]^{\mathrm{T}} \end{aligned} \tag{1}$$

$$\mathbf{R}(\psi) = \begin{bmatrix} \cos\psi & -\sin\psi & 0 \\ \sin\psi & \cos\psi & 0 \\ 0 & 0 & 1 \end{bmatrix} \tag{2}$$

where x and y are the Cartesian coordinates of the center of mass of the AUV in {**I**}, ψ denotes the yaw angle in {**I**},

and u, v, and r denote the surge, sway, and yaw velocities, respectively, expressed in {**B**}.

Based on the momentum theorem, the AUV's dynamic model in the horizontal plane is expressed as in a previous study [33], as follows:

$$\begin{aligned} m[\dot{u} - vr] &= \frac{\rho}{2}l^4 X'_{rr} r^2 + \frac{\rho}{2}l^3[X'_{\dot{u}}\dot{u} + X'_{vr}vr] \\ &\quad + \frac{\rho}{2}l^2[X'_{uu}u^2 + X'_{\delta}u^2\delta] + \tau_u \\ m[\dot{v} + ur] &= \frac{\rho}{2}l^4[Y'_{\dot{r}}\dot{r} + Y'_{r|r|}r\,|r|] + \frac{\rho}{2}l^3[Y'_{\dot{v}}\dot{v} \\ &\quad + Y'_r ur] + \frac{\rho}{2}l^2[Y'_v uv + Y'_{v|v|}v\,|v| + Y'_{\delta}u^2\delta] \\ I_z\dot{r} &= \frac{\rho}{2}l^5[N'_{\dot{r}}\dot{r} + N'_{r|r|}r\,|r|] + \frac{\rho}{2}l^4[N'_{\dot{v}}\dot{v} + N'_r ur \\ &\quad + N'_{|v|r}\,|v|\,r] + \frac{\rho}{2}l^3[N'_v uv + N'_{v|v|}v\,|v| + N'_{\delta}u^2\delta] \end{aligned} \tag{3}$$

Here, I_z is the moment of inertia about the vertical axis, m is the mass of the vessel, ρ is the density of the surrounding fluid, and l is the length of AUV. The control input τ_u is the force produced by thruster. X'_{δ}, Y'_{δ}, and N'_{δ} denote the dimensionless coefficients of forces and moments generated by a couple of vertical rudders. Meanwhile, $X'_{\dot{u}}$, X'_{rr}, X'_{vr}, X'_{uu}, $Y'_{r|r|}$, $Y'_{\dot{r}}$, $Y'_{\dot{v}}$, Y'_r, Y'_v, $Y'_{v|v|}$, $N'_{\dot{r}}$, $N'_{r|r|}$, $N'_{\dot{v}}$, N'_r, $N'_{|v|r}$, N'_v, and $N'_{v|v|}$ are the dimensionless hydrodynamic coefficients of the AUV, as shown in Table 2. The hydrodynamic parameters are determined from planar motion mechanism (PMM) tests in a circulating water tunnel.

The lift and draft coefficient curves of the rudders C_L and C_D are obtained by tank experiments, and are related to effective fin angle of attack α, as shown in Fig. 3 [34]. Then, the dimensionless coefficients of forces and moments generated by rudders can be calculated according to their definitions [33], as shown in Table 3.

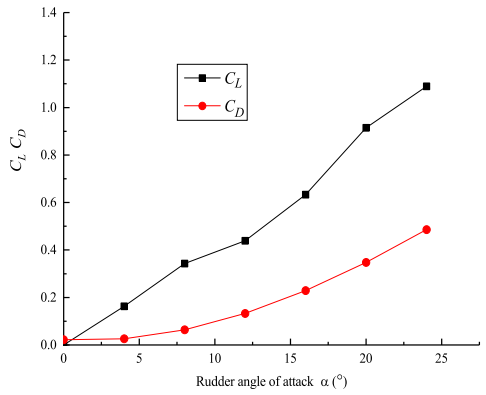

FIGURE 3. Relationship curve of α, C_L, and C_D.

In 1975, Nomoto using the automatic regulation principle to analyze the heading response equation of underactuated marine vehicles, and then the first-order Nomoto model was put forward:

$$T\dot{r} + r = K\delta \tag{4}$$

TABLE 3. Dimensionless coefficients of forces and moments generated by rudders.

Parameters	Value
X'_{δ}	$-5.962\cdot10^{-3}$
N'_{δ}	$5.554\cdot10^{-3}$
Y'_{δ}	$-1.336\cdot10^{-2}$

where K is the static yaw rate gain, and T is the effective yaw rate time constant. K and T can be written as follows:

$$\begin{aligned} T &= -\left(\frac{l}{u}\right)\left[\frac{(I'_z - N'_{\dot{r}})Y'_v + (N'_r - N'_{\delta})(m' - Y'_{\dot{v}})}{C_H} \right. \\ &\quad \left. + \frac{(m' - Y'_{\dot{v}})N'_{\delta}}{C_N}\right] \\ K &= \left(\frac{u}{l}\right)\frac{C_N}{C_H} \\ C_H &= N'_r Y'_v + N'_v(m' - Y'_r), \quad C_N = Y'_{\delta}N'_v - N'_{\delta}Y'_v \end{aligned} \tag{5}$$

The parameter l is a constant. Thus, the parameters T and K can be rewritten as follows:

$$T = T_0 \cdot \left(\frac{u_0}{u}\right), \quad K = K_0 \cdot \left(\frac{u}{u_0}\right) \tag{6}$$

Here, u is the surge velocity of the AUV, and

$$\begin{aligned} T_0 &= -\left(\frac{l}{u_0}\right)\left[\frac{(I'_z - N'_{\dot{r}})Y'_v + (N'_r - N'_{\delta})(m' - Y'_{\dot{v}})}{C_H} \right. \\ &\quad \left. + \frac{(m' - Y'_{\dot{v}})N'_{\delta}}{C_N}\right] \\ K_0 &= \left(\frac{u_0}{l}\right)\frac{C_N}{C_H} \end{aligned} \tag{7}$$

Therefore, once the parameters T_0 and K_0 at a certain velocity u_0 are obtained by (7) or manipulability tests, the parameters at other velocities can be updated with (6).

B. TOC FOR FIRST-ORDER NOMOTO MODEL

According to (4), the problem of time-optimal control for heading motion can be described as follows:

$$\begin{aligned} J &= \int_0^{t_f} 1dt = t_f \\ s.t. &\begin{cases} \dot{x}_1(t) = -x_2(t) \\ \dot{x}_2(t) = -\dfrac{1}{T}x_2(t) + \dfrac{K}{T}\delta(t) \\ \boldsymbol{x}(0) = \boldsymbol{x}_0, \boldsymbol{x}(t_f) = 0, \quad |\delta| \le \delta_{\max} \end{cases} \end{aligned} \tag{8}$$

where δ denotes the rudder angle with maximum value $\delta_{\max}$, $x_1(t) = \psi_e(t) = \psi_d - \psi(t)$ is the heading error, and $x_2(t) = r(t)$ is the angular velocity of heading.

The essence of time-optimal control is to find a control law $\delta(t)$ that minimizes the time from the initial state of plant $\boldsymbol{x}_0$ to zeros. The Hamiltonian function for (8) is given by the following:

$$\begin{aligned} H(x(t), \delta(t), \lambda(t), t) &= 1 - \lambda_1(t)x_2(t) \\ &\quad + \lambda_2(t)(-\frac{1}{T}x_2(t) + \frac{K}{T}\delta(t)) \end{aligned} \tag{9}$$

Hence, the co-state equation can be written as follows:

$$\begin{aligned}\dot{\lambda}_1 &= -\frac{\partial H}{\partial x_1} = 0\\ \dot{\lambda}_2 &= -\frac{\partial H}{\partial x_2} = \lambda_1(t) + \frac{1}{T}\lambda_2(t)\end{aligned} \tag{10}$$

By solving the differential (10), $\lambda_1(t)$ and $\lambda_2(t)$ can be determined as follows:

$$\begin{aligned}\lambda_1(t) &= C_1\\ \lambda_2(t) &= -C_1T + C_2e^{t/T}\end{aligned} \tag{11}$$

where C_1 and C_2 are constants.

According to the maximum principle, in order to achieve the global minimum for H, the control law is taken as the following:

$$\delta_{TC} = \begin{cases}\delta_{\max} & \lambda_2(t) < 0\\ -\delta_{\max} & \lambda_2(t) > 0\end{cases} \tag{12}$$

From (12), it is seen that the system state can reach the origin by changing the sign of the control signal at most once.

Substituting $\delta = \delta_{\max}$ into (8) gives the following expressions for the phase locus:

$$\begin{aligned}&\frac{1}{T}x_1 - x_2 - K\delta_{\max}\ln\frac{x_2 - K\delta_{\max}}{C_3'} = C_4'\\ &C_3' = x_{20} - K\delta_{\max}, \quad C_4' = \frac{1}{T}x_{10} - x_{20}\end{aligned} \tag{13}$$

Equation (12) represents a family of curves, which means that any state of the plant will move along the family of curves under the action of the control variable $\delta = \delta_{\max}$. The part of the curve (passing through the origin) with $x_2 \le 0$ (Fig. 4) is the switching curve l_1, which indicates that any state (x_1, x_2) on l_1 can reach the origin under the action $\delta = \delta_{\max}$:

$$l_1 : x_1 - Tx_2 - KT\delta_{\max}\ln(1 - \frac{x_2}{K\delta_{\max}}) = 0 \quad x_2 \le 0 \tag{14}$$

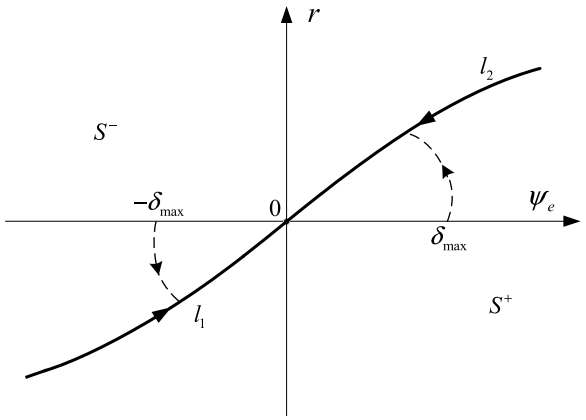

FIGURE 4. Switching curve of time-optimal control.

Similarly, the switching curve l_2 (Fig. 4) is obtained with the action $\delta = -\delta_{\max}$. Then, the complete time-optimal switching curve l_T by combining l_1 and l_2 can be written as follows:

$$l_T : x_1 = Tx_2 - KT\delta_{\max}\mathrm{sgn}(x_2)\ln(1 + \frac{|x_2|}{K\delta_{\max}}) \tag{15}$$

Finally, the TOC control law for heading control of the underactuated AUV is given by the following:

$$\delta_{TC} = \begin{cases}\delta_{\max}(\psi_e, r) \in S^+ \cup l_1\\ -\delta_{\max}(\psi_e, r) \in S^- \cup l_2\end{cases} \tag{16}$$

Remark 1: The rationale of the TOC control is that for the initial state within region S^+, the saturated control signal $\delta = \delta_{\max}$ is applied to drive the system state intersection with l_2. Then, the sign of the control signal is changed to $\delta = -\delta_{\max}$, and at last the system state arrives at the origin in finite time along curve l_2. The system state can arrive at the origin with the similar control procedures when the initial state is within region S^-.

We can rewrite the control law as follows:

$$\begin{aligned}\delta_{TC} &= \delta_{\max}\cdot\mathrm{sgn}(\psi_e + f_T(r))\\ f_T(r) &= -Tr + \mathrm{sgn}(r)KT\delta_{\max}\ln(1 + \frac{|r|}{K\delta_{\max}})\end{aligned} \tag{17}$$

C. PROBLEM FORMULATION

The designed TOC control law based on the accurate first-order Nomoto model is impossible to implement in practical heading motion systems. Therefore, the following problems must be considered.

1. How to consider the unmodeled dynamics and external disturbances when designing the TOC control law for the nonlinear heading dynamic model (3)?
2. How to make the control signal change sign accurately on the switching curve and make the system state decay gracefully to zero?
3. How to deal with the parameters change of the heading dynamic model at different velocities?

III. CONTROLLER DESIGN

The heading controller is designed in two steps. First, a model-compensation ADRC (MC-ADRC) is developed, the nonlinear heading dynamic model is compensated for by a first-order Nomoto model through using model-compensation ESO. Moreover, a parameter self-tuning strategy is designed for MC-ADRC by the controller scaling method. Then, the soft-switching PTOC (SPTOC) is proposed, the TOC with an unsaturated region (RTOC) is designed by using a switching region to replace the switching curve, and a soft-switching strategy is proposed to achieve the smooth switching between RTOC and the PD controller based on the Takagi–Sugeno fuzzy mode. Figure 5 shows the structure of the soft-switching proximate time-optimal heading control system.

A. SELF-TUNING MODEL-COMPENSATION ADRC

According to reference [22], we propose a model-compensation ADRC (MC-ADRC) for heading control.

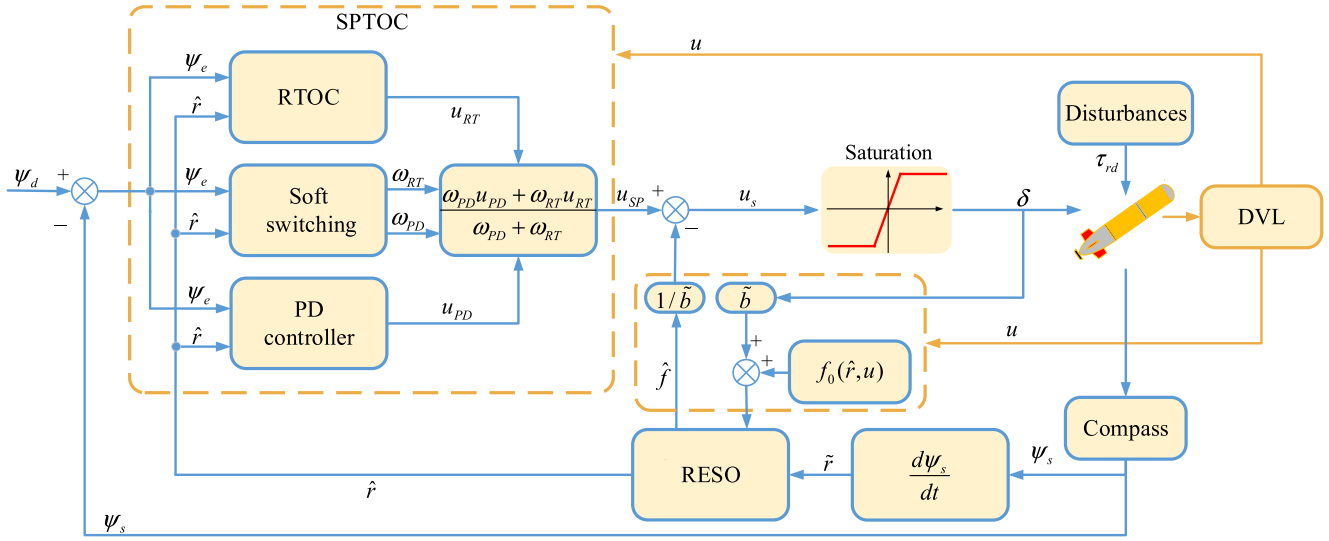

FIGURE 5. Structure of the soft-switching proximate time-optimal heading control system.

The outstanding characteristic of MC-ADRC is that the nonlinear heading dynamic model (3) is compensated to a first-order Nomoto model rather than a double integral system through using a model-compensation ESO (MC-ESO). Figure 6 shows the structure of the controller.

Based on (3) and (4), the nonlinear heading dynamic model can be rewritten as follows:

$$\begin{cases} \dot{\psi} = r \\ \dot{r} = f(r,u,v,\dot{v},\tau_{rd},\delta) + \tilde{b}\delta \\ \quad = f_0(r,u) + f_1(r,u,v,\dot{v},\tau_{rd},\delta) + \tilde{b}\delta \end{cases} \tag{18}$$

where $\tilde{b}$ denotes the control gain and is the estimated value of b. $f(r,u,v,\dot{v},\tau_{rd},\delta) = f_0(r,u) + f_1(r,u,v,\dot{v},\tau_{rd},\delta)$, and $f_0(r,u)$ is the known partial model, and $f_1(r,u,v,\dot{v},\tau_{rd},\delta)$ is the unknown part of the model.

Remark 2: In (18), $f_0(r,u) = -r/\tilde{T}$, $\tilde{T}$ is the estimated value of T, and the expression is based on the Nomoto model; $f_1(r,u,v,\dot{v},\tau_{rd},\delta)$ is the total disturbance [18], which includes the unknown internal dynamics, the external disturbances τ_{rd}, and the equivalent disturbances caused by the control gain b and the uncertainty of model parameter T. In ADRC, f_1 is treated as an extended state of the heading motion system, and is estimated and compensated by an extended state observer (ESO).

According to (4) and (6), the control gain b is given by the following:

$$b = \frac{K}{T} = \left(\frac{u}{u_0}\right)^2 \cdot \frac{K_0}{T_0} = u^2 \cdot b_0 \tag{19}$$

where $b_0 = K_0/(T_0 \cdot u_0^2)$.

Remark 3: In (19), assuming that the velocity u can be measured by the *Linkquest NavQuest*600 DVL mounted on the WL-3 AUV. This DVL will only output valid velocity measurements when the water column below the vehicle is higher than 30 cm and less than 140 m; the standard depth rating of the DVL is 800 m. Recently, parameter identification technology for AUV has made some progress [35], and the model parameters b_0 and T_0 can be accurately estimated. Therefore, once the parameters b_0 and T_0 at a certain velocity u_0 are obtained, the parameters at other velocities can be updated with (19) and (6).

This ESO of regular ADRC for heading motion is of three orders, and there is a redundancy since the first component of the state ψ_s can be measured directly. Thus, the reduced-order ESO (RESO) (proposed in [36], [37]) is adopted in this paper to reduce complexity and the number of adjustable parameters. Angular velocity r and total disturbances f_1 are estimated by RESO, and can be expressed as follows:

$$\begin{cases} \tilde{r} = d\psi_s/dt \\ e = \hat{r} - \tilde{r} \\ \dot{\hat{r}} = \hat{f} - \beta_1 \cdot fal(e,\alpha_1,\sigma_1) + \tilde{b} \cdot sat(u_s) \\ \dot{\hat{f}} = -\beta_2 \cdot fal(e,\alpha_2,\sigma_2) \end{cases} \tag{20}$$

where ψ_s is the actual heading angle, $\hat{r}$ is the estimated values of the AUV states r, $\hat{f}$ is an extended state that is used to estimate the total disturbances f_1, β_i is the gain coefficient, and $sat(\cdot)$ denotes the saturation function.

In (20), $fal(e,\alpha,\sigma)$ is a power function with a linear region, and it can be expressed as follows:

$$fal(e,\alpha,\sigma) = \begin{cases} |e|^{\alpha}\,\mathrm{sgn}(e) & |e| > \sigma \\ \dfrac{e}{\sigma^{1-\alpha}} & |e| \le \sigma \end{cases} \tag{21}$$

where α and σ are the adjustable parameters.

Many researchers have made progress on the parameters tuning of ESO, and there are quantities of useful engineering experiences and theoretical analysis results for parameters tuning [38].

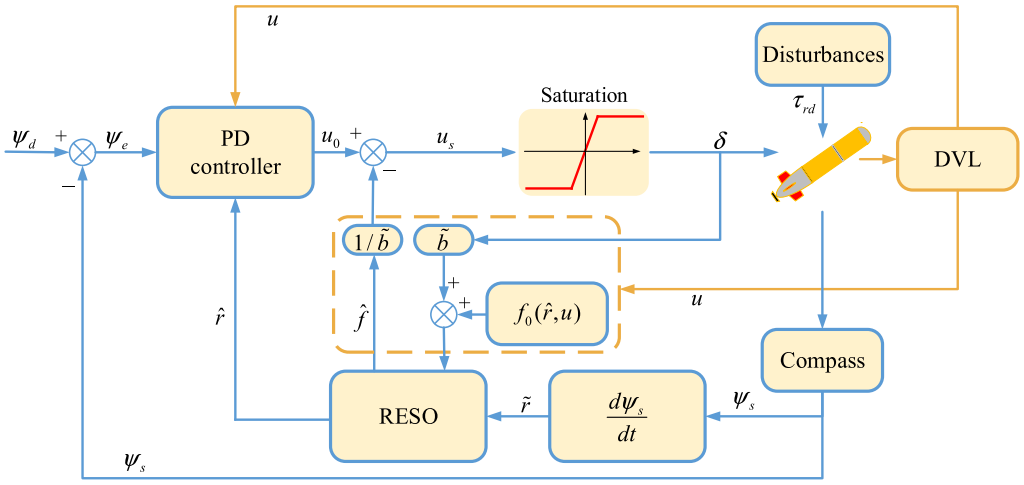

FIGURE 6. Structure of self-tuning model-compensation ADRC (MC-ADRC) for heading control.

Based on the design principle of RESO, if the known partial model $f_0(\hat{r}, u)$ can be added to the third equation of RESO, the disturbances estimated by $\hat{f}$ will decrease. Therefore, the estimation accuracy and efficiency of RESO can be improved, and the new MC-RESO can be written as follows:

$$\begin{cases} \tilde{r} = d\psi_s/dt \\ e = \tilde{r} - \hat{r} \\ \dot{\hat{r}} = \hat{f} - \beta_1 \cdot fal(e, \alpha_1, \sigma_1) - \dfrac{1}{\tilde{T}}\hat{r} + \tilde{b} \cdot \delta \\ \dot{\hat{f}} = -\beta_2 \cdot fal(e, \alpha_2, \sigma_2) \end{cases} \tag{22}$$

where $\delta = sat(u_s)$.

When $\hat{f} \approx f_1$, the control law for plant (18) is designed as:

$$u_s = u_0 - \frac{\hat{f}}{\tilde{b}} \tag{23}$$

Therefore, the plant model (18) can be approximately transformed into the first-order Nomoto model:

$$\begin{cases} \dot{\psi} = r \\ \dot{r} \approx -\dfrac{1}{\tilde{T}}r + \tilde{b}u_0 \end{cases} \tag{24}$$

A proportional-derivative (PD) controller can be designed to control this model:

$$u_0 = k_p\psi_e - k_d\hat{r} \tag{25}$$

where k_p and k_d are the control parameters, $\psi_e = \psi_d - \psi_s$, ψ_d denotes the target heading, ψ_s is the actual heading, $\hat{r}$ is the estimation of angular velocity, and u_0 is the output of the PD controller.

A controller-parameter self-tuning strategy for heading control of underactuated AUV at different velocities is then designed based on the controller scaling method in [39]. The transfer function of the plant (24) is given by the following:

$$G_p(s) = \frac{K_r}{\frac{s}{\omega_p}(\frac{s}{\omega_p} + 1)} \tag{26}$$

where

$$\begin{aligned} K_r &= \tilde{T}^2\tilde{b} \\ \omega_p &= 1/\tilde{T} \end{aligned} \tag{27}$$

Then, the feedback gains of the PD controller can be selected as follows:

$$k_p = \frac{\bar{k}_p}{K_r}, \quad k_d = \frac{\bar{k}_d}{K_r\omega_p} \tag{28}$$

Once the model parameters (b_0 and T_0) and controller parameters ($\bar{k}_p$ and $\bar{k}_d$) at a certain velocity u_0 are obtained, the self-tuning MC-ADRC can be established by updating the parameters of MC-RESO and the PD controller at other velocities with the following equations:

$$\begin{aligned} \tilde{b} &= b_0\left(\frac{u}{u_0}\right)^2, \quad \tilde{T} = T_0\left(\frac{u_0}{u}\right) \\ k_p &= \frac{\bar{k}_p}{b_0T_0^2}, \quad k_d = \frac{\bar{k}_d}{b_0T_0}\left(\frac{u_0}{u}\right) \end{aligned} \tag{29}$$

where u is the surge velocity of the AUV measured by the DVL.

B. PROXIMATE TIME-OPTIMAL CONTROL (PTOC)

The TOC control law for heading in (17) is not feasible because even the smallest system noise would make the control system chatter. Such behavior is the result of the infinite slope of the function $f_T(r)$ at $r = 0$, and is obviously unacceptable in a practical control system. The purpose of the PTOC is to eliminate this behavior while maintaining nearly minimum time [27].

The first step in the implementation of PTOC for heading control is to define a "slab" region around the switching curve in TOC control law where control remains unsaturated. The maximum rudder angle is used until the system state enters this unsaturated region wherein the system actively tracks a nearly optimal curve until the heading error is small.

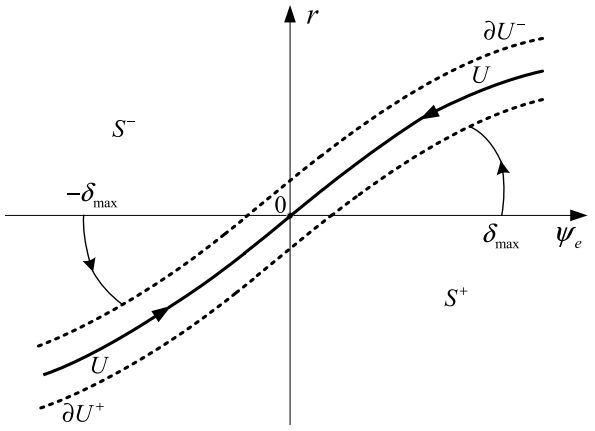

FIGURE 7. Operating regions of RTOC for heading control.

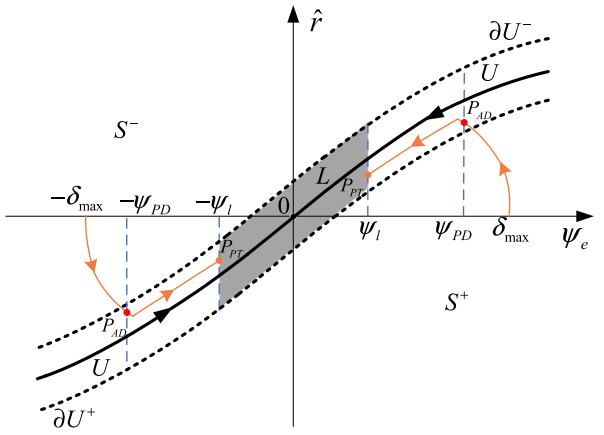

FIGURE 8. Operating regions of PTOC and ADRC for heading control.

Therefore, the switching curve of TOC with an unsaturated region (RTOC) can be obtained from the time-optimal switching curve l_T given in Section II by adding a heading error offset term to the positive or negative portions of the switching curve. The control law RTOC can be written as follows [32]:

$$\delta = \delta_{\max} \cdot sat[\gamma \cdot (f_s(r) + \psi_e)] \tag{30}$$

where $\gamma > 0$ denotes the parameter of the switching region. $f_s(r)$ is given by the following:

$$f_s(r) = sign(r) \cdot (\tilde{T}^2 \tilde{b} \delta_{\max} \ln(1 + \frac{|r|}{\tilde{T}\tilde{b}\delta_{\max}}) - y_s) - \tilde{T} r \tag{31}$$

where y_s denotes an offset for heading error and its expression is $y_s = \delta_{\max}/\gamma$.

The operating regions for RTOC are shown in Fig. 7. The following three regions can be defined in the state space of the RTOC, including control saturation regions S^+ and S^- and unsaturated region U:

$$\begin{aligned} S^- &= \left\{(\psi_e, r) \in \mathbb{R}^2 : [\gamma \cdot (f_s(r) + \psi_e)] < -1\right\} \\ S^+ &= \left\{(\psi_e, r) \in \mathbb{R}^2 : [\gamma \cdot (f_s(r) + \psi_e)] > 1\right\} \\ U &= \left\{(\psi_e, r) \in \mathbb{R}^2 : |\gamma \cdot (f_s(r) + \psi_e)| \le 1\right\} \end{aligned} \tag{32}$$

In [30] and [32], a robust PTOC control law was designed, the unmeasured velocity and unknown disturbance were estimated by RESO for feedback and compensation, and the effectiveness was verified. In this paper, the MC-RESO is adopted to design robust RTOC for the heading control of the AUV; this can be expressed as follows:

$$\begin{aligned} u_{RT} &= \delta_{\max} \cdot sat[\gamma \cdot (f_s(\hat{r}) + \psi_e)] \\ \delta &= sat(u_{RT} - \frac{\hat{f}}{\tilde{b}}) \end{aligned} \tag{33}$$

where $\hat{r}$ and $\hat{f}$ are the estimates of angular velocity and total disturbances by MC-RESO.

Then, the system state enters a linear region $|\psi_e| \le \psi_l$, and the response decays accurately to zero with an ESO-based feedback control law. The controller designed in the preceding section can be expressed as follows:

$$\begin{aligned} u_{PD} &= k_p \psi_e - k_d \hat{r} \\ \delta &= sat(u_{PD} - \frac{\hat{f}}{\tilde{b}}) \end{aligned} \tag{34}$$

where k_p and k_d are the feedback gains of heading error and angular velocity. ψ_l is the limit of the linear region.

Remark 4: Figure 8 shows the partial phase locus of ADRC with saturation constraints and PTOC, and points P_{AD} and P_{PT} denote the intersection of the phase locus and PD control region for ADRC and PTOC, respectively. Comparing to

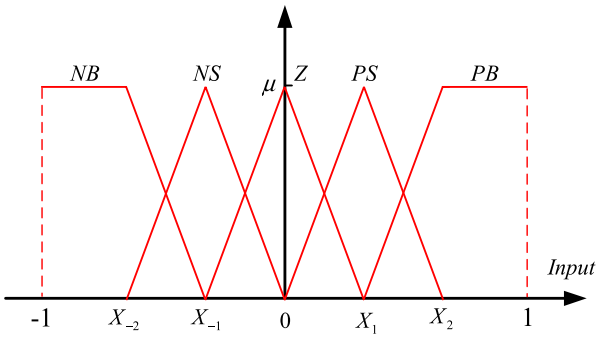

FIGURE 9. Fuzzy logic membership functions of heading error ψ_e and angular velocity $\hat{r}$.

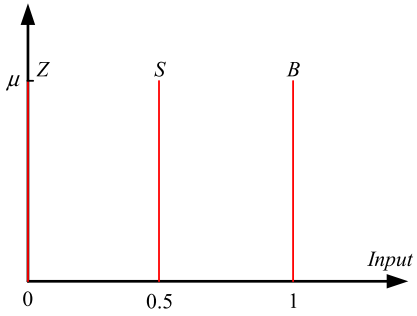

FIGURE 10. Fuzzy logic membership functions for strength coefficient of the PD controller ω_{PD} and PTOC controller ω_{PT}.

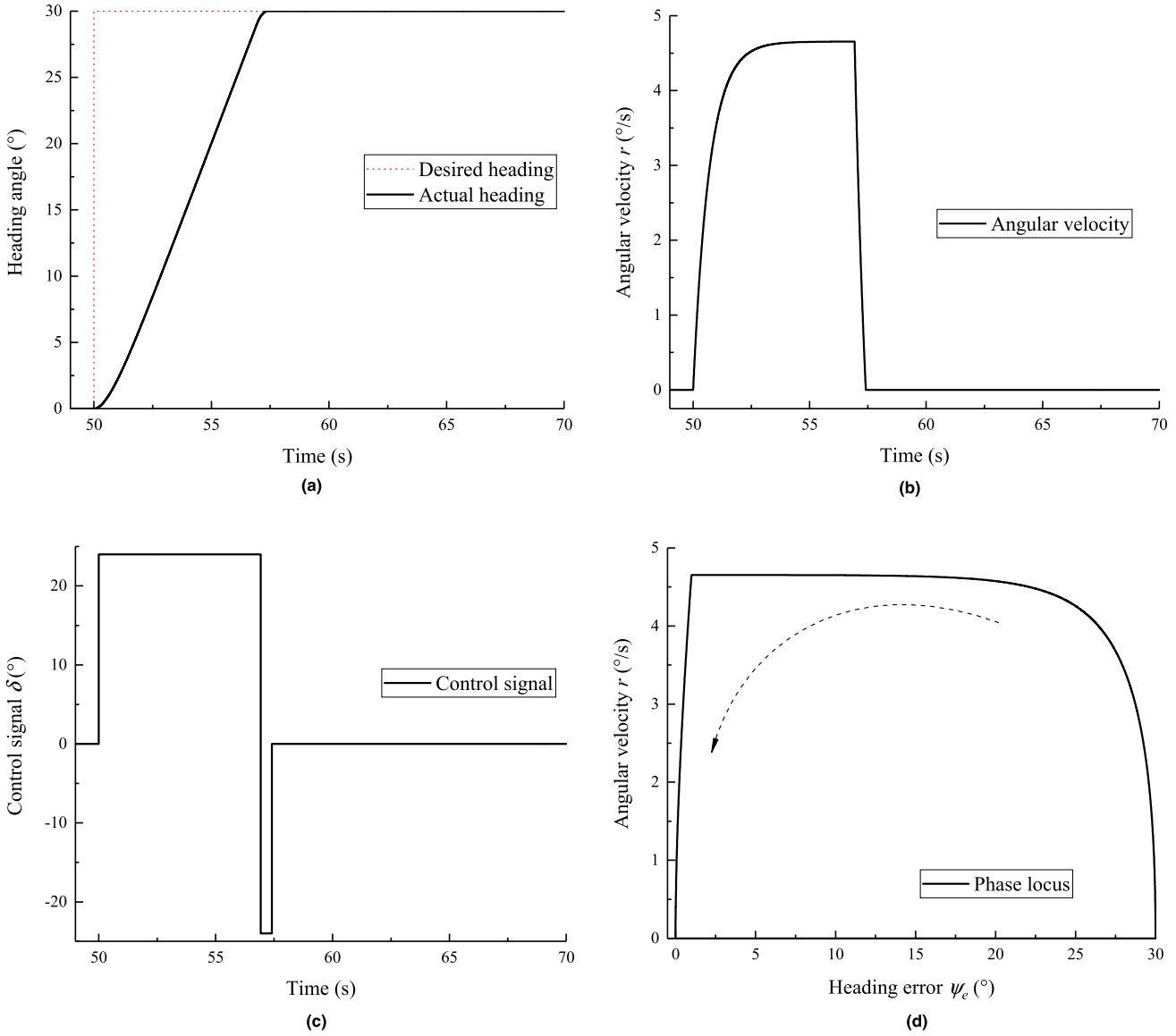

FIGURE 11. Heading control results of TOC for first-order Nomoto model. (a) Heading angle response. (b) Angular velocity response. (c) Output of control signal. (d) Phase locus of TOC for heading control.

ADRC, PTOC has a smaller PD control region because PTOC has eliminated most heading error with RTOC before the system state enters the linear region L. Therefore, the parameters of the PD controller in PTOC need to be readjusted, and are quite different from those of ADRC.

Note: ψ_{PD} denotes the limit of the PD control region for ADRC.

C. SOFT-SWITCHING BASED ON TAKAGI–SUGENO FUZZY MODE

The switching strategy for RTOC and the PD controller in PTOC is usually threshold switching, and the controllers satisfy the constraints of continuity and smoothness at the switching point. It is obviously unreasonable that the threshold is constant for different targets and at different surge velocities. In order to solve the problem of threshold switching, a soft-switching scheme based on the Takagi–Sugeno fuzzy mode is proposed for the PD and the RTOC controller. The structure of soft-switching is illustrated in Fig. 5.

In a T-S fuzzy system, the antecedent parts (IF) of IF–THEN rules are identical to the typical Mamdani fuzzy systems, but the consequent part (THEN) is a linear combination of the input variables. Thus, a T-S fuzzy system can be described as a mean weight of the obtained values from THEN parts of the rules [40], [41]. In this paper, the inputs of the fuzzy switching mode are selected as the heading error ψ_e and the angular velocity $\hat{r}$, and the outputs are the strength coefficients of the PD controller ω_{PD} and RTOC controller ω_{RT}. The practical domain of heading error is $[-\psi_{e0}, \psi_{e0}]$, and $\psi_{e0} > 0$ is given by the following:

$$\psi_{e0} = |\psi_d - \psi_{s0}| \tag{35}$$

where ψ_{s0} is the heading angle when ψ_d changes.

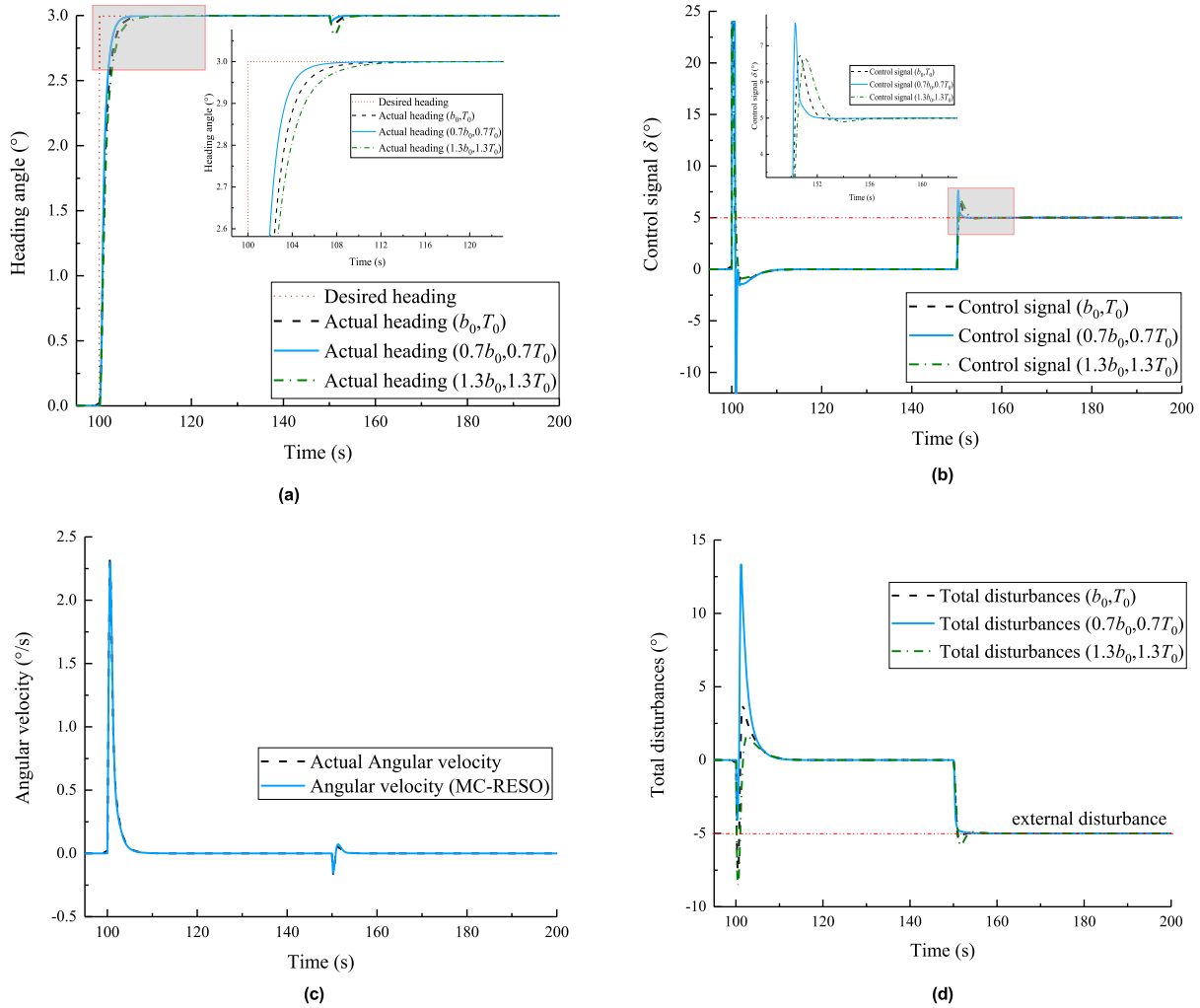

FIGURE 12. Heading control results of MC-ADRC with parameter perturbation. (a) Heading angle response. (b) Output of control signal. (c) Actual and estimated of angular velocity ($\tilde{b} = b_0, \tilde{T} = T_0$). (d) Estimate of total disturbances.

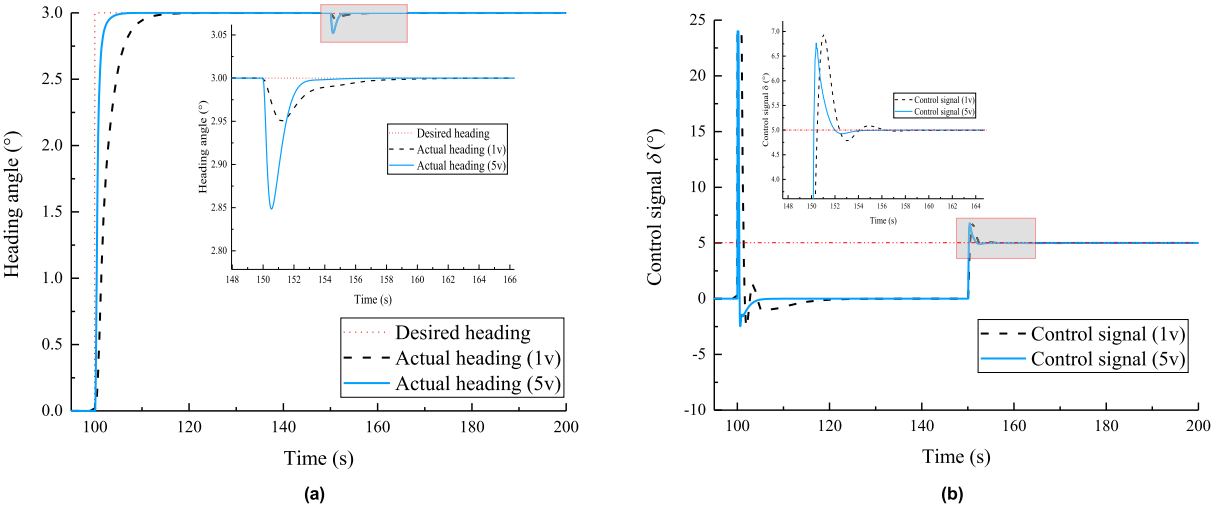

FIGURE 13. Simulation results of self-tuning MC-ADRC. (a) Heading angle response. (b) Output of control signal.

The practical domain of angular velocity is $[-r_{\max}, r_{\max}]$, and $r_{\max} > 0$ denotes the maximum angular velocity of the AUV. It can be expressed as in a previous study [31], as follows:

$$r_{\max} = \frac{u}{u_0} \cdot r_{\max 0} \tag{36}$$

where $r_{\max 0}$ is the maximum angular velocity at velocity u_0.

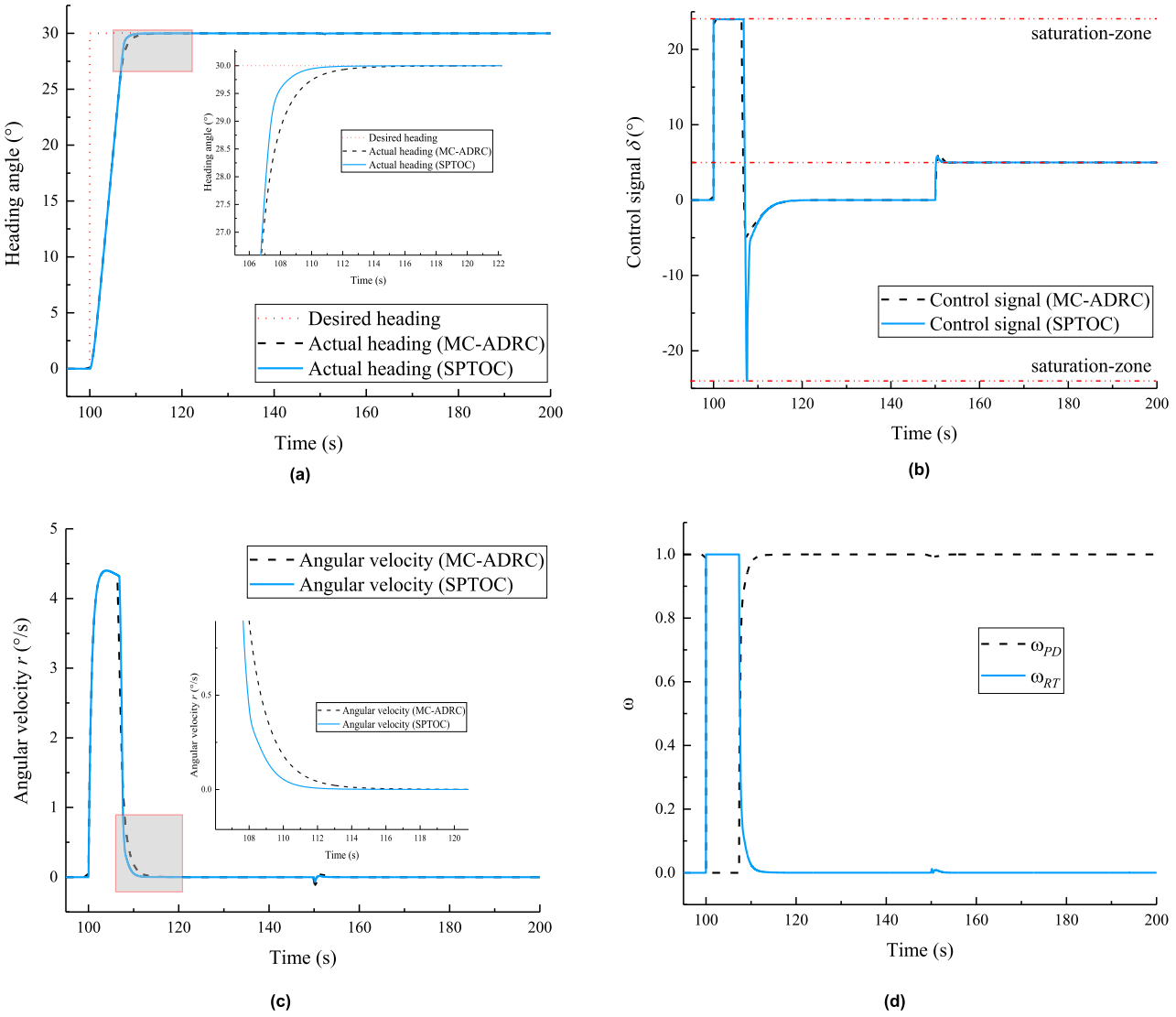

FIGURE 14. Heading control results of SPTOC and MC-ADRC (*Volt* = 3V). (a) Heading angle response. (b) Output of control signal. (c) Angular velocity response. (d) Strength coefficients of controllers.

For the input variable including heading error and angular velocity, the fuzzy domain is set as $[-1, 1]$ by scale transformation for the practical domain, and the quantization factor is $1/\psi_{e0}$ and $1/r_{\max}$; the linguistic variables are selected as $\{NB, NS, Z, PS, PB\}$, the membership function is triangular, and $(X_{-2}, X_{-1}, 0, X_1, X_2)$ denotes the position of the membership function maximum, as shown in Fig. 9. The positions of the membership function maximum for heading error and angular velocity are set as $(-0.3, -0.15, 0, 0.15, 0.3)$ and $(-0.5, -0.25, 0, 0.25, 0.5)$.

For the output variable including the strength coefficients of the PD and RTOC controller, the fuzzy domain is set as $[0, 1]$ and is the same as the practical domain. The linguistic variables are selected as $\{Z, S, B\}$, and the output of the membership function is a unit constant. These functions are shown in Fig. 10.

The fuzzy rules to compute ω_{PD} and ω_{RT} are listed in Table 4 and Table 5.

TABLE 4. The fuzzy control rules for ω_{PD}.

ω_{PD} \ ψ_e / $\hat{r}$	*NB*	*NS*	*Z*	*PS*	*PB*
NB	0	0	–	–	–
NS	0	0.5	0.5	–	–
Z	0	0.5	1	0.5	0
PS	–	–	0.5	0.5	0
PB	–	–	–	0	0

Defuzzification was performed using the weighted average (wtaver) method. Then, a SPTOC control law is proposed based on soft-switching can be expressed as

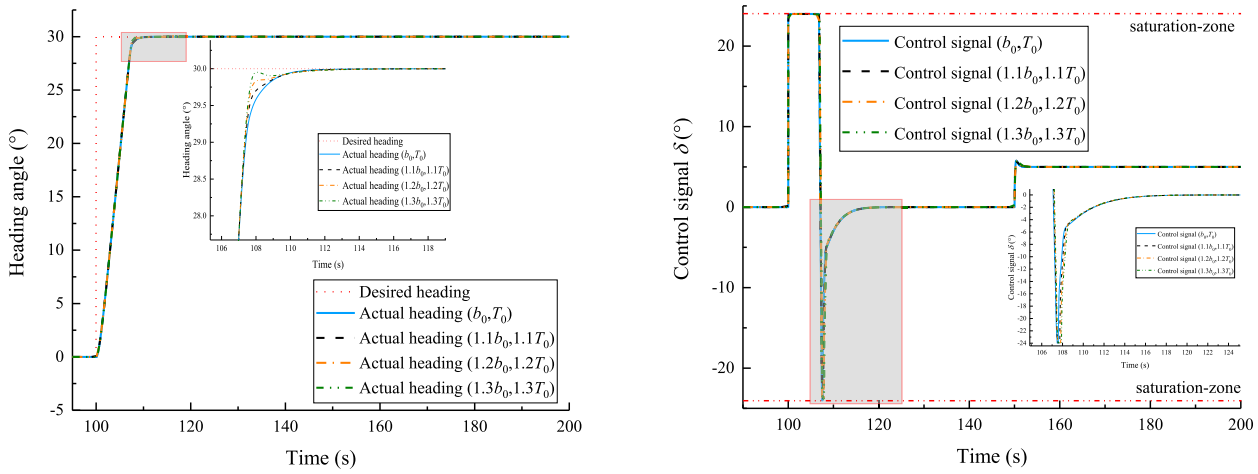

FIGURE 15. Heading control results of SPTOC with parameter perturbation. (a) Heading angle response. (b) Output of control signal.

TABLE 5. The fuzzy control rules for ω_{RT}.

ω_{RT} / ψ_e / $\hat{r}$	NB	NS	Z	PS	PB
NB	1	1	–	–	–
NS	1	0.5	0.5	–	–
Z	1	0.5	0	0.5	1
PS	–	–	0.5	0.5	1
PB	–	–	–	1	1

follows:

$$u_{sp} = \frac{\omega_{PD}u_{PD} + \omega_{RT}u_{RT}}{\omega_{PD} + \omega_{RT}} \tag{37}$$

where u_{sp} is the output of the SPTOC controller.

IV. SIMULATIONS

In order to verify and demonstrate the effectiveness of the proximate time-optimal heading control schemes proposed for the underactuated AUV, several simulations are carried out on the WL-3 AUV with a maximum rudder angle $\delta_{\max} = 24°$. By ignoring the second-order terms in (3), the parameters K_0 and T_0 are estimated with (38): $K_0 = 0.194$, and $T_0 = 0.695$. Therefore, the parameters K_0 and T_0 retain a level of uncertainty, as follows:

$$T_0 = \frac{(N'_{\dot{r}} - I'_z)l}{N'_r u_0}, \quad K_0 = (-\frac{N'_\delta u_0}{N'_r l}) \tag{38}$$

Here, $u_0 = 2$ kn is the cruising velocity.

A. TOC FOR FIRST-ORDER NOMOTO MODEL

The first-order Nomoto model with the parameters K_0 and T_0 is adopted to build the simulation system in MATLAB Simulink, and the control law is TOC with expression (17). The initial heading angle and angular velocity of the AUV is $\begin{bmatrix}\psi_0 & r_0\end{bmatrix} = \begin{bmatrix}0° & 0°/s\end{bmatrix}$, and the desired heading angle is $\psi_d = 30°(t \geq 50s)$.

Due to the discretization of the sampling period, it is difficult for the control signal to switch on the switching curve, and the system state may not arrive at the origin accurately, thus causing oscillation. Therefore, the sampling period is set as $T_S = 0.001\ s$, and the stopping condition of TOC is relaxed. Thus, the TOC control law is rewritten as follows:

$$\delta_{TC} = \begin{cases} 0 & \psi_e \leq 5 \cdot 10^{-3°} \\ & \& \ r \leq 5 \cdot 10^{-9°/s} \\ \delta_{\max} \cdot \mathrm{sgn}(\psi_e + f(r)) & \text{others} \end{cases} \tag{39}$$

The obtained simulation results are shown in Fig. 11.

From Fig. 11, the result shows that the TOC control law designed in Section II is feasible for heading control of AUV. The system state can reach to the neighborhood of origin by changing the sign of control signal once, and the adjusting time (2% error bound) is 7.026 s, and the changing of control signal happens at 6.927 s with the system state $\begin{pmatrix}\psi_e, r\end{pmatrix} = \begin{pmatrix}0.997°, 4.654°/s\end{pmatrix}$, which provides a reference for the switching strategy design in PTOC.

B. SELF-TUNING MODEL-COMPENSATION ADRC FOR HEADING CONTROL

The dynamic model in (3) (with the parameters listed in Table 2) is adopted to build the simulation system in MATLAB Simulink. Two different simulations are carried out here to verify the effectiveness and reliability of the designed MC- ADRC heading control algorithm.

Case 1: The input voltage of the propeller is set to 3 V. The initial heading angle and angular velocity of the AUV is $\begin{bmatrix}\psi_0 & r_0\end{bmatrix} = \begin{bmatrix}0° & 0°/s\end{bmatrix}$, and the desired heading angle is $\psi_d = 3°(t \geq 100\ s)$. The control gain and known model parameters are $\tilde{b} = b_0 = K_0/T_0 = 0.28$, and $\tilde{T} = T_0$.

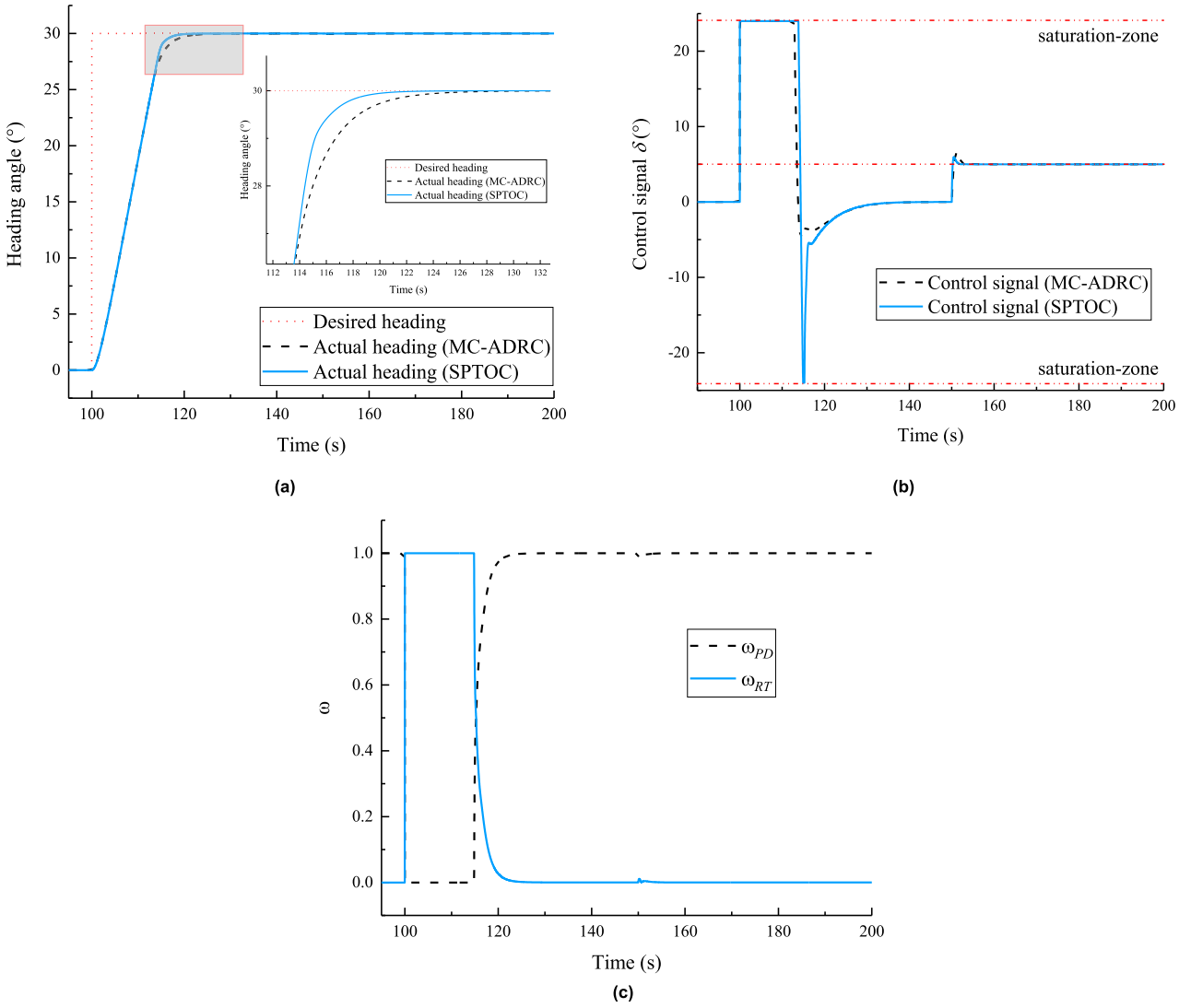

FIGURE 16. Heading control results of SPTOC and MC-ADRC (*Volt* = 1V). (a) Heading angle response. (b) Output of control signal. (c) Strength coefficients of controllers.

TABLE 6. Parameters of the MC-ADRC controller.

Parameters	Value	Parameters	Value
$\bar{k}_p$	2.97	$\bar{k}_d$	4.17
β_{01}	6	β_{02}	1.5
α_1	0.5	σ_1	0.05
α_2	0.25	σ_2	0.05

The disturbance is $\tau_{rd} = \tilde{b} \cdot (-5°)\,(t \geq 150\,s)$. The control parameters are adjusted to ensure that there is no overshoot. The main initial parameters of MC-ADRC are listed in Table 6.

In order to verify the robustness of the MC-ADRC controller, the control gain and known model parameters have 30% parameter perturbation: $\tilde{b} = 0.7b_0, \tilde{T} = 0.7T_0$ and $\tilde{b} = 1.3b_0, \tilde{T} = 1.3T_0$. The parameters of MC-ADRC in Table 4 are still adopted. The obtained simulation results are shown in Fig. 12.

Case 2: The input voltage of the propeller is set to 1 V and 5 V. The initial heading angle and angular velocity of the AUV is $\left[\,\psi_0 \;\; r_0\,\right] = \left[\,0° \;\; 0°/s\,\right]$, and the desired heading angle is $\psi_d = 3°(t \geq 100\,s)$. The parameter self-tuning strategy is implemented based on (29). The obtained simulation results are shown in Fig. 13.

As shown in Fig. 12, MC-ADRC is effective for the heading control of underactuated AUV with external disturbances and parameter perturbations. When the uncertainties of control gain $\tilde{b}$ and known model parameter $\tilde{T}$ reach 30%, the performance of the controller is scarcely influenced. Fig. 12(b) shows that the control signal under external disturbances is smooth and continuous, which indicates that the control law is reasonable and effective. From Fig. 12(c) and Fig. 12(d),

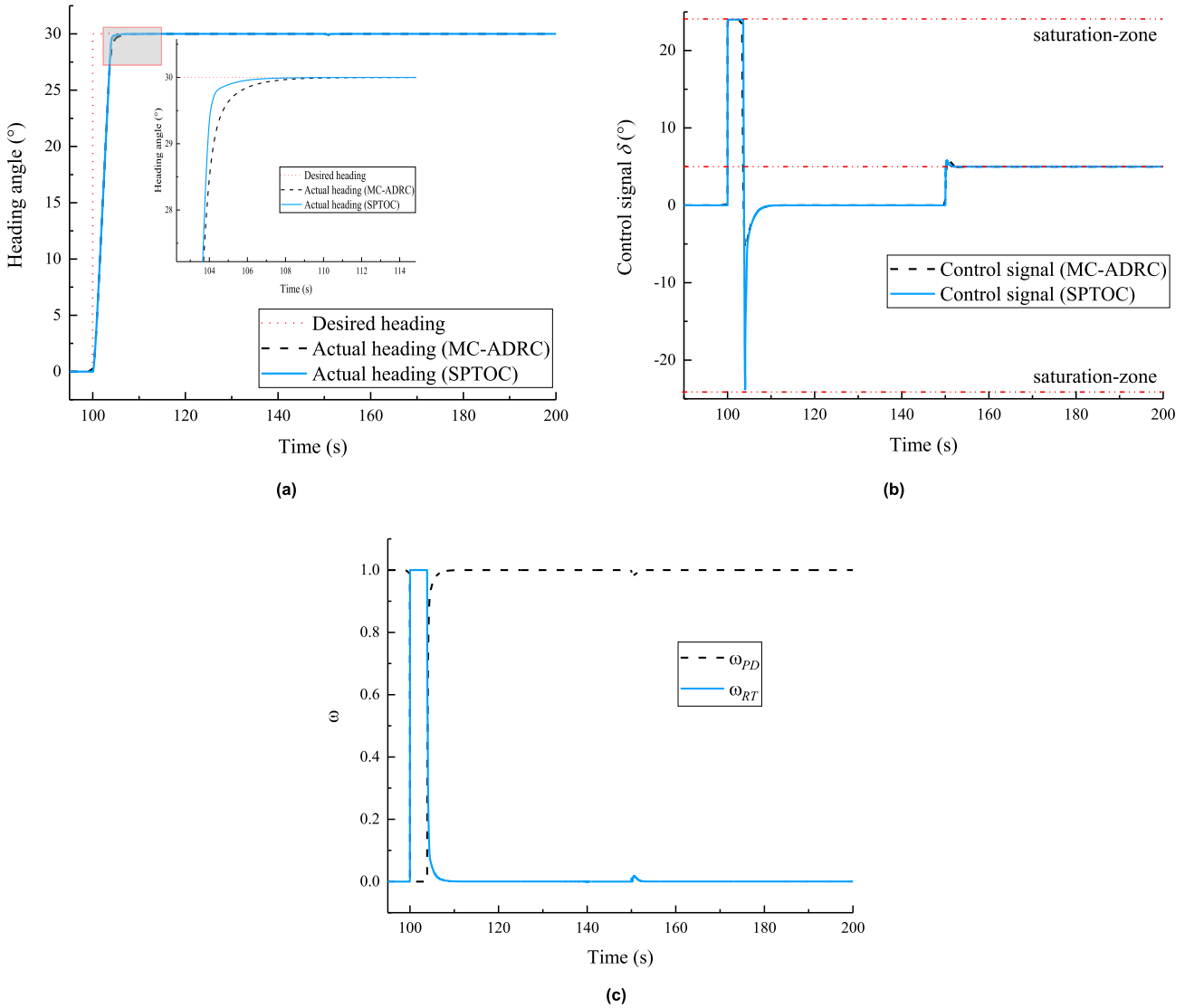

FIGURE 17. Heading control results of SPTOC and MC-ADRC (*Volt* = 5V). (a) Heading angle response. (b) Output of control signal. (c) Strength coefficients of controllers.

it appears that the angular velocity of AUV can be accurately estimated by MC-RESO throughout the process, and it takes about 3 s ($\tilde{b} = b_0, \tilde{T} = T_0$) for the MC-RESO to produce a decent estimation of external disturbance, which indicates that the MC-RESO designed in Section III is efficient and accurate.

Meanwhile, Fig. 13 shows that the self-tuning MC-ADRC is effective for the heading control of underactuated AUV at different velocities. Figure 13(a) shows that, under different thruster input voltages (1 V, 5 V), all heading controllers have good performance and no overshoot, which indicates that the self-adjustment strategy is effective. Figure 13(b) shows that the external disturbance can be accurately estimated and compensated by the control system.

C. SOFT-SWITCHING PTOC FOR HEADING CONTROL

In order to verify the proposed schemes and demonstrate the effectiveness of soft-switching PTOC for the heading control of underactuated AUV, several simulations are carried out, and the effectiveness is verified by comparisons with self-tuning MC-ADRC. The simulation system built in the preceding section is used here.

Case 1: The input voltage of the propeller is set to 3 V. The initial heading angle and angular velocity of the AUV is $\begin{bmatrix} \psi_0 & r_0 \end{bmatrix} = \begin{bmatrix} 0° & 0°/s \end{bmatrix}$, and the desired heading angle is $\psi_d = 30°(t \geq 100\ s)$. The control gain and known model parameters are $\tilde{b} = b_0, \tilde{T} = T_0$, and the disturbance is $\tau_{rd} = \tilde{b} \cdot (-5°)\,(t \geq 150\ s)$. The control parameters are adjusted to ensure that there is no overshoot for SPTOC. The main initial parameters of SPTOC are listed in Table 7, and the parameters of RESO in Table 6 are adopted.

The obtained simulation results are shown in Fig. 14.

Then, in order to verify the robustness of SPTOC, a simulation is carried out with parameter perturbations of 10%, 20%, and 30%; the parameters of SPTOC in Table 7 are still adopted. The obtained simulation results are shown in Fig. 15.

TABLE 7. Parameters of the SPTOC controller.

Parameters	Value
γ	20
$r_{\max 0}$	$5°/s$
$\bar{k}_p$	20.43
$\bar{k}_d$	16

TABLE 8. Performance comparison in adjusting time (s), with $\psi_d = 30°(t = 100s)$.

Propeller input voltage	1 V	3 V	5 V
MC-ADRC (T_{AD})	17.96	8.84	4.57
SPTOC (T_{SP})	15.98	7.7	4.03
Improvement (%) $(\frac{T_{AD}-T_{SP}}{T_{AD}})$	11	12.9	11.8

Note: T_{AD} and T_{SP} denote the adjusting time of MC-ADRC and SPTOC, respectively.

Case 2: The input voltage of the propeller is set to 1 V and 5 V. The initial heading angle and angular velocity of the AUV is $\begin{bmatrix} \psi_0 & r_0 \end{bmatrix} = \begin{bmatrix} 0° & 0°/s \end{bmatrix}$, and the desired heading angle is $\psi_d = 30°(t \geq 100\ s)$; the disturbance is $\tau_{rd} = \tilde{b} \cdot (-5°)\,(t \geq 150\ s)$. The parameter $r_{\max}$ is updated based on (36), and k_p and k_d are updated based on (29). The obtained simulation results are shown in Fig. 16 for $Volt = 1$V and Fig. 17 for $Volt = 5$V.

From Figs. 14, 16, and 17, it can be found that SPTOC is effective for the heading control of underactuated AUV at different velocities. The strength coefficients of controllers are continuous and smooth, which indicates that the switching PD controller and RTOC controller are stationary. The external disturbance can be accurately estimated and compensated by the SPTOC control system. Figure 15 shows that with the increase in parameter perturbation the performance of SPTOC in the switching region worsens. Therefore, SPTOC needs higher accuracy for model parameters compared with MC-ADRC. Table 8 summarizes the performance in terms of adjusting time (2% error bound) with no overshoot. Obviously, the SPTOC can track the target heading more quickly than the MC-ADRC at all velocities in the simulations.

V. CONCLUSION

A soft-switching proximate time-optimal control (PTOC) is proposed in this paper, based on MC-ESO and Takagi–Sugeno fuzzy switching, for the fast set-heading tracking of underactuated AUV. Several simulations are carried out to verify the effectiveness of the designed controller, and the following conclusions can be drawn.

1. Based on Pontryagin's maximum principle, a time-optimal heading control law is derived for the underactuated AUV heading with a first-order Nomoto model. The simulation results show that the TOC control law is feasible only when the plant model is accurate and the stopping condition is relaxed.

2. A MC-ESO is introduced to the heading dynamic, the unmeasured velocity and unknown total disturbances is estimated by MC-ESO for feedback and compensation. A parameter self-tuning strategy is developed for MC-ADRC to improve the adaptability of the controller with the changed dynamic model. The effectiveness of the self-tuning MC-ADRC is proved by the simulations at different velocities.

3. Soft-switching PTOC is designed, and the Takagi–Sugeno fuzzy mode is adopted to realize the soft-switching between ADRC (near the origin) and RTOC (far from the origin). Compared with the MC-ADRC algorithm, the proposed SPTOC needs higher accuracy for model parameters and shows better performance in the simulations compared with MC-ADRC.

In the future, we will try to apply the MC-ADRC and SPTOC algorithms proposed in this paper to the path following control of the AUV, and further study the parameter adjustment of SPTOC and fuzzy switching strategy.

REFERENCES

[1] M. H. Khodayari and S. Balochian, "Modeling and control of autonomous underwater vehicle (AUV) in heading and depth attitude via self-adaptive fuzzy PID controller," *J. Mar. Sci. Technol.*, vol. 20, no. 3, pp. 559–578, 2015.

[2] J. Wan, B. He, Y. Shen, W. Liu, X. Ding, and S. Gao, "Heading multimode control based on soft-switching for autonomous underwater vehicle," *Ocean Eng.*, vol. 164, pp. 672–682, Sep. 2018.

[3] N. Palomeras, G. Vallicrosa, A. Mallios, J. Bosch, E. Vidal, N. Hurtos, M. Carreras, and P. Ridao, "AUV homing and docking for remote operations," *Ocean Eng.*, vol. 154, pp. 106–120, Apr. 2018.

[4] M. H. Khooban, N. Vafamand, T. Dragičević, and F. Blaabjerg, "Polynomial fuzzy model-based approach for underactuated surface vessels," *IET Control Theory Appl.*, vol. 12, no. 7, pp. 914–921, 2018.

[5] Y. Li, L. Wang, Y. Liao, Q. Jiang, and K. Pan, "Heading MFA control for unmanned surface vehicle with angular velocity guidance," *Appl. Ocean Res.*, vol. 80, pp. 57–65, Nov. 2018.

[6] R. E. Precup, M. B. Rădac, S. Preitl, E. M. Petriu, and J. Fodor, "On the optimal design of low-cost fuzzy controllers for ship course control," in *Proc. Int. Symp. Electron. Mar. (ELMAR)*, Sep. 2009, pp. 163–166.

[7] Z. Dong, L. Wan, Y. Li, T. Liu, J. Zhuang, and G. Zhang, "Point stabilization for an underactuated AUV in the presence of ocean currents," *Int. J. Adv. Robot. Syst.*, vol. 12, no. 7, p. 100, 2015.

[8] M. Caccia, M. Bibuli, R. Bono, and G. Bruzzone, "Basic navigation, guidance and control of an unmanned surface vehicle," *Auto. Robots*, vol. 25, no. 4, pp. 349–365, Nov. 2008.

[9] Y. Li, Y.-Q. Jiang, L.-F. Wang, J. Cao, and G.-C. Zhang, "Intelligent PID guidance control for AUV path tracking," *J. Central South Univ.*, vol. 22, no. 9, pp. 3440–3449, 2015.

[10] Y. Li, Y. Jiang, J. Cao, B. Wang, and Y. Li, "AUV docking experiments based on vision positioning using two cameras," *Ocean Eng.*, vol. 110, pp. 163–173, Dec. 2015.

[11] J. Yuan, Z. Wu, J. Yu, and M. Tan, "Sliding mode observer-based heading control for a gliding robotic dolphin," *IEEE Trans. Ind. Electron.*, vol. 64, no. 8, pp. 6815–6824, Aug. 2017.

[12] K. Tanakitkorn, P. A. Wilson, S. R. Turnock, and A. B. Phillips, "Sliding mode heading control of an overactuated, hover-capable autonomous underwater vehicle with experimental verification," *J. Field Robot.*, vol. 35, no. 3, pp. 396–415, 2018.

[13] K. Teo, B. Goh, and O. K. Chai, "Fuzzy docking guidance using augmented navigation system on an AUV," *IEEE J. Ocean. Eng.*, vol. 40, no. 2, pp. 349–361, Apr. 2015.

[14] J. Du, X. Hu, M. Krstić, and Y. Sun, "Robust dynamic positioning of ships with disturbances under input saturation," *Automatica*, vol. 73, pp. 207–214, Nov. 2016.
[15] Z. Dong, T. Bao, M. Zheng, X. Yang, L. Song, and Y. Mao, "Heading control of unmanned marine vehicles based on an improved robust adaptive fuzzy neural network control algorithm," *IEEE Access*, vol. 7, pp. 9704–9713, 2019.
[16] N.-K. Im and V.-S. Nguyen, "Artificial neural network controller for automatic ship berthing using head-up coordinate system," *Int. J. Nav. Archit. Ocean Eng.*, vol. 10, no. 3, pp. 235–249, 2018.
[17] X. Yang, J. Cui, D. Lao, D. Li, and J. Chen, "Input shaping enhanced active disturbance rejection control for a twin rotor multi-input multi-output system (TRMS)," *ISA Trans.*, vol. 62, pp. 287–298, May 2016.
[18] J. Han, "From PID to active disturbance rejection control," *IEEE Trans. Ind. Electron.*, vol. 56, no. 3, pp. 900–906, Mar. 2009.
[19] R.-C. Roman, R.-E. Precup, E. M. Petriu, and F. Dragan, "Combination of data-driven active disturbance rejection and Takagi-Sugeno fuzzy control with experimental validation on tower crane systems," *Energies*, vol. 12, no. 8, p. 1548, Apr. 2019.
[20] R. Wang, S. Wang, Y. Wang, C. Tang, and M. Tan, "Three-dimensional helical path following of an underwater biomimetic vehicle-manipulator system," *IEEE J. Ocean. Eng.*, vol. 43, no. 2, pp. 391–401, Apr. 2018.
[21] R. Cui, L. Chen, C. Yang, and M. Chen, "Extended state observer-based integral sliding mode control for an underwater robot with unknown disturbances and uncertain nonlinearities," *IEEE Trans. Ind. Electron.*, vol. 64, no. 8, pp. 6785–6795, Aug. 2017.
[22] S. Li, K. Zhang, J. Li, and C. Liu, "On the rejection of internal and external disturbances in a wind energy conversion system with direct-driven PMSG," *ISA Trans.*, vol. 61, pp. 95–103, Mar. 2016.
[23] B. Saerens, M. Diehl, and E. van den Bulck, "Optimal control using Pontryagin's maximum principle and dynamic programming," in *Automotive Model Predictive Control*, L. del Re, F. Allgöwer, L. Glielmo, C. Guardiola, and I. Kolmanovsky, Eds. London, U.K.: Springer, 2010, pp. 119–138.
[24] J.-Y. Park, B.-H. Jun, P.-M. Lee, J.-H. Oh, and Y.-K. Lim, "Underwater docking approach of an under-actuated AUV in the presence of constant ocean current," *IFAC Proc. Volumes* vol. 43, no. 20, pp. 5–10, 2010.
[25] M. Workman, R. L. Kosut, and G. F. Franklin, "Adaptive proximate time-optimal servomechanisms: Continuous time case," in *Proc. Amer. Control Conf.*, vol. 3, Jun. 1987, pp. 589–594.
[26] M. L. Workman, R. L. Kosut, and G. F. Franklin, "Adaptive proximate time-optimal servomechanisms: Discrete-time case," in *Proc. 26th IEEE Conf. Decis. Control*, Dec. 1987, pp. 1548–1553.
[27] A. Dhanda and G. F. Franklin, "An improved 2-DOF proximate time optimal servomechanism," *IEEE Trans. Magn.*, vol. 45, no. 5, pp. 2151–2164, May 2009.
[28] Y. Choi, J. Jeong, and D. Gweon, "A novel damping scheduling scheme for proximate time optimal servomechanisms in hard disk drives," *IEEE Trans. Magn.*, vol. 42, no. 3, pp. 468–472, Mar. 2006.
[29] A. T. Salton, Z. Chen, and M. Fu, "Improved control design methods for proximate time-optimal servomechanisms," *IEEE/ASME Trans. Mechatronics*, vol. 17, no. 6, pp. 1049–1058, Dec. 2012.
[30] G. Cheng and J.-G. Hu, "An observer-based mode switching control scheme for improved position regulation in servomotors," *IEEE Trans. Control Syst. Technol.*, vol. 22, no. 5, pp. 1883–1891, Sep. 2014.
[31] T. I. Fossen, *Handbook of Marine Craft Hydrodynamics and Motion Control*. Hoboken, NJ, USA: Wiley, 2011.
[32] T. Lu and G. Cheng, "Expanded proximate time-optimal servo control of permanent magnet synchronous motor," *Optim. Control Appl. Methods*, vol. 37, no. 4, pp. 782–797, Jul. 2016.
[33] T. Prestero, "Verification of a six-degree of freedom simulation model for the REMUS autonomous underwater vehicle," Massachusetts Inst. Technol., Cambridge, MA, USA, Tech. Rep., 2001.
[34] X. Liang, Y. Li, Z. Peng, and J. Zhang, "Nonlinear dynamics modeling and performance prediction for underactuated AUV with fins," *Nonlinear Dyn.*, vol. 84, no. 1, pp. 237–249, 2016.
[35] M. T. Sabet, H. M. Daniali, A. Fathi, and E. Alizadeh, "Identification of an autonomous underwater vehicle hydrodynamic model using the extended, cubature, and transformed unscented Kalman filter," *IEEE J. Ocean. Eng.*, vol. 43, no. 2, pp. 457–467, Aug. 2018.
[36] G. Tian, "Reduced-order extended state observer and frequency response analysis," Cleveland State Univ., Cleveland, OH, USA, Tech. Rep., 2007.
[37] J.-B. Yu and Y.-Q. Wu, "Global robust tracking control for a class of cascaded nonlinear systems using a reduced-order extended state observer," *Nonlinear Dyn.*, vol. 94, no. 2, pp. 1277–1289, 2018.
[38] W. Xue and Y. Huang, "Tuning of sampled-data ADRC for nonlinear uncertain systems," *J. Syst. Sci. Complex.*, vol. 29, no. 5, pp. 1187–1211, Oct. 2016.
[39] Z. Gao, "Scaling and bandwidth-parameterization based controller tuning," in *Proc. Amer. Control Conf.*, vol. 6, Jun. 2003, pp. 4989–4996.
[40] O. Naghash, V. Fereshtehpoor, M. Hassan, and F. Blaabjerg, "Analysis, control and design of a non-inverting buck-boost converter: A bumpless two-level T–S fuzzy PI control," *ISA Trans.*, vol. 67, pp. 515–527, Mar. 2017.
[41] N. Vafamand, M. H. Asemani, A. Khayatiyan, M. H. Khooban, and T. Dragicevic, "TS fuzzy model-based controller design for a class of nonlinear systems including nonsmooth functions," *IEEE Trans. Syst., Man, Cybern. Syst.*, to be published.

AN LI received the B.S. degree in naval architecture and ocean engineering from Harbin Engineering University, Harbin, China, in 2011, where he is currently pursuing the Ph.D. degree of design and manufacture of marine structure.

His research interests include autonomous underwater vehicles, modeling, dynamic analysis, and control of autonomous underwater vehicles.

LI YE received the B.S. degree in shipbuilding engineering from Harbin Engineering University, Harbin, China, in 2001, and the M.S. and Ph.D. degrees in design and manufacture of marine structure from Harbin Engineering University, in 2004 and 2007, respectively.

He is currently a Professor with Harbin Engineering University. His research interests include autonomous underwater vehicles, navigation, and motion control of autonomous underwater vehicles.

JIANG YANQING received the M.S. and Ph.D. degrees in design and manufacture of marine structure major from Harbin Engineering University, in 2013 and 2016, respectively.

He held a Postdoctoral position at the University of Southampton, from 2017 to 2018. He is currently a Lecturer with Harbin Engineering University. His research interests include navigation, and guidance and control of unmanned underwater vehicles.

LI YUEMING received the B.S. degree in naval architecture and ocean engineering from Harbin Engineering University, China, in 2005, and the M.S. and Ph.D. degrees in design and manufacture of marine structure from Harbin Engineering University, Harbin, China, in 2004 and 2007, respectively.

He is currently an Associate Research Fellow with Harbin Engineering University. His research interests include autonomous underwater vehicles, control of autonomous underwater vehicles, and cooperative control of multi-AUVS.

CAO JIAN received the B.S. degree in naval architecture and ocean engineering from Harbin Engineering University, China, in 2007, and the Ph.D. degree in design and manufacture of marine structure from Harbin Engineering University, Harbin, China, in 2013.

He is currently a Lecturer with Harbin Engineering University. His research interests include overall design and performance calculation of autonomous underwater vehicles, and control of autonomous underwater vehicles.

HE JIAYU received the B.S. degree in naval architecture and ocean engineering from the Harbin Engineering University, Harbin, China, in 2011, where he is currently pursuing the Ph.D. degree in design and manufacture of marine structure.

His research interests include autonomous underwater vehicles, AUV fault diagnosis, and nonlinear state estimation.